PROCEEDINGS B

royalsocietypublishing.org/rspb

Research

Cite this article: Chatterjee M *et al*. 2026 *araucan* regulates butterfly wing iridescence by coordinating scale structure and pigmentation. *Proc. R. Soc. B* **293**: 20252984.
https://doi.org/10.1098/rspb.2025.2984

Received: 18 November 2025
Accepted: 17 March 2026

Subject Category:
Genetics and genomics

Subject Areas:
genetics, developmental biology, evolution

Keywords:
structural coloration, iridescence, butterfly wing patterns, *Iroquois*-complex, evo-devo

Authors for correspondence:
Martik Chatterjee
e-mails: martikchatterjee@gmail.com; mc2548@cornell.edu
Robert Reed
e-mail: robertreed@cornell.edu

†These authors contributed equally to the study.

Electronic supplementary material is available online at https://doi.org/10.6084/m9.figshare.c.8420607.

THE ROYAL SOCIETY PUBLISHING

araucan regulates butterfly wing iridescence by coordinating scale structure and pigmentation

Martik Chatterjee[1,2,3], Cedric Finet[4], Kate J. Siegel[1,2], Shen Tian[3,†], Yifei Joye Zhou[3,†], Ling Shen Loh[5,†], Xin Yi Yu[1,2,†], Seydeanna Delgado[1,†], Jeanne M. C. Mcdonald[1], Anyi Mazo-Vargas[3], Antonia Monteiro[4] and Robert Reed[1]

[1]Department of Ecology and Evolutionary Biology, and [2]Department of Molecular Biology and Genetics, Cornell University, Ithaca, NY, USA
[3]Department of Biology, Duke University, Durham, NC, USA
[4]Department of Biological Sciences, Faculty of Science, National University of Singapore, Singapore
[5]Department of Biological Sciences, The George Washington University, Washington, DC, USA

MC, 0000-0003-4689-6212; AM, 0000-0001-9696-459X; RR, 0000-0002-6065-6728

Butterfly wings exhibit a remarkable diversity of structural iridescent colours, yet the genetic regulation of iridescence remains poorly understood. Here, we show that the *Iroquois*-complex transcription factor gene *araucan* plays a role in modulating wing scale iridescence in the common buckeye butterfly, *Junonia coenia*. Using CRISPR-Cas9 knockouts, we demonstrate that loss of *araucan* function causes dorsal wing scales to shift from golden-brown to blue iridescence, and eyespot centre scales to shift from saturated purple-violet to dull grey-brown. These phenotypes are associated with increased lower lamina thickness (LL) in dorsal cover scales and decreased LL in eyespot-centre cover and ground scales, effects known to influence thin-film interference iridescence, along with reduced pigmentation in eyespot ground scales. Together, these results identify *araucan* as a single transcription factor that determines colouration by simultaneously regulating both photonic architecture and light-absorbing pigmentation and show that these effects can be regulated in a pattern-specific manner. Our findings provide a framework for linking gene regulation to the spatially coordinated evolution of structural and pigmentary components of colour.

1. Introduction

colouration in animals serves as a powerful model for understanding how gene regulatory networks give rise to complex, adaptive traits. Colour is most commonly generated by light-reflecting pigments, by structural features that alter light reflectance or through a combination of both. Although structural colouration is widespread across the animal kingdom—particularly in insects—its genetic and developmental bases remain poorly understood [1]. Butterfly wings, with their nanostructured scales and vivid structural organization that produce blue, purple and green hues, offer a useful system for uncovering how genes shape the physical traits that underlie these colours.

Over the past decade, advances in genomic mapping and CRISPR-Cas9 gene editing have enabled the discovery and functional validation of key genes and regulatory elements involved in butterfly wing pigmentation and patterning. Comparative studies and insights from model insects such as *Drosophila melanogaster* have also helped inform developmental genetic models of wing pattern determination. However, the genetic basis of

structural colouration still remains weakly resolved, with only a handful of key regulatory genes identified across a few butterfly species. These include *optix*, a regulator of blue iridescence in *Junonia coenia* [2,3] and silver scale development in *Speyeria mormonia* [4]; *bric-a-brac* and *doublesex*, which control UV-reflecting scales in *Colias* spp. [5] and *Zerene* spp. [6], and *antennapedia*, *apterousA*, *doublesex*, *ultrabithorax*, *optix* and *hr38*, which regulate silver reflectance in *Bicyclus anynana* [7,8]. Of these examples, *optix* is the only gene so far characterized to regulate lower lamina thickness , a thin-film mechanism underlying blue structural iridescence in wing scales [2,3].

Here, we investigate the role of *araucan/caupolican* (also known as *iroquois2*), an *Iroquois*-complex transcription factor gene, in the wing patterning of the common buckeye butterfly *J. coenia*. Most hexapods, including butterflies, possess two *Iroquois* genes —one orthologous to *D. melanogaster's mirror* (*iroquois1*) and one to *araucan/caupolican* (*iroquois2*). In *D. melanogaster, iroquois2* has undergone a lineage-specific duplication, giving rise to the paralogues *araucan* and *caupolican* [9–11]. The three *Iroquois* genes (*araucan*, *caupolican* and *mirror*) in *D. melanogaster* regulate multiple developmental processes, including dorsal notum patterning, longitudinal wing vein specification and posterior wing domain (alula) identity [12–16]. Recent findings suggest that *mirror* specifies a far posterior domain in butterfly wings—a role probably ancestral in broad-winged insects but lost in *D. melanogaster* and other calyptrate flies owing to evolutionary reductions in wing complexity [11]. Despite its expression in the basal part of the wing in *Heliconius* butterflies [17], the function of *araucan/caupolican* (hereafter *araucan*) in butterflies has thus far remained untested.

In this study, we used CRISPR-Cas9 mutagenesis and gene expression analyses to investigate the role of *araucan* in wing colouration in *J. coenia*. We show that *araucan* is a regulator of both wing-scale ultrastructure, including the iridescence-determining LL and scale pigmentation. Our findings identify *araucan* as a novel regulator of colouration in butterflies that functions via a process of coordinated pigment and structural effects. This work provides, to our knowledge, the first functional evidence for this gene outside of *D. melanogaster*, highlighting its evolutionary flexibility and specialized role in modulating scale-based structural colour traits.

2. Material and methods

(a) Identification of *Iroquois*-complex genes

We previously identified the *Iroquois*-complex genes in *J. coenia* [11]. For this study, we used an updated annotation [18], which resulted in revised gene model identifiers for the *Iroquois* complex. We generated a phylogeny using inferred full-length predicted amino acid sequences of the *Iroquois*-complex genes (electronic supplementary material, file S1) and identified the *J. coenia* gene *JC_g12213* as the single orthologue of *D. melanogaster araucan/caupolican* paralogues (electronic supplementary material, figure S1). For clarity and consistency, we refer to *JC_g12213* as *araucan* in *J. coenia*, with the understanding that it is equally related to both of its paralogues in *D. melanogaster*. The updated phylogeny and sequence information used for orthology assignments are provided in the electronic supplementary material, figure S1 and file S1, respectively. To ensure reproducibility and compatibility with future genome and annotation releases, we have provided both the predicted amino acid and coding DNA sequences of *araucan* in the electronic supplementary material, file S1.

(b) CRISPR-Cas9 mutagenesis of *araucan* in *Junonia coenia*

To assess the function of *araucan* in *J. coenia,* we generated CRISPR-Cas9 somatic mosaic deletions targeting the *araucan* coding region. We used a previous protocol where early embryos are injected with single guide RNAs (sgRNAs) and Cas9 enzyme [19]. Mutations induced in early syncytial embryos typically only affect a subset of nuclei, resulting in mosaic knockout (mKO) animals.

We designed two sgRNAs—5′-CTGGGTACGATTTAGCAGCC-3′ and 5′-CTCCTGCTCCTTGTCCTCGT-3′—to target the exon of *araucan* containing the conserved homeobox domain in *J. coenia* (electronic supplementary material, figure S1a). Possible off-target sgRNAs were ruled out by BLAST searching against the *J. coenia* genome assembly. sgRNAs were synthesized by Integrated DNA Technologies, Inc. (Coralville, IA, USA), rehydrated in 1× Tris-EDTA buffer and mixed with Alt-R S.p. Cas9 Nuclease/Nickase (Integrated DNA Technologies, Inc.) to a final concentration of 200 ng ul^{-1} sgRNA and 500 ng ul^{-1} Cas9.

We collected eggs by placing *Plantago lanceolata* leaves in a cage with gravid females for 1–2 h and then prepared eggs for microinjection by submersing them in 5% benzalkonium chloride (Sigma-Aldrich, St Louis, MO, USA) for 30 s followed by a wash with distilled water. Prepared eggs were then lined up on double-sided tape on glass slides and sgRNA and Cas9 mixture was injected into the eggs using a 0.5 mm borosilicate needle (Sutter Instruments, Novato, CA, USA) and a PLI-100 Picoinjector (Harvard Apparatus, Holliston, MA, USA). Injections were completed within 2–3 h after oviposition, and larvae from injected eggs were raised on an artificial diet at 27 °C, 70% humidity, and a 16 h : 8 h light : dark cycle. Adults were frozen upon emergence and phenotyped and imaged using a Keyence VHX-7000 microscope.

(c) Genotyping CRISPR mutants

We genotyped *J. coenia* mKO mutants to confirm Cas9-induced deletions in the *araucan* gene. We selected mutant individuals mKO 'A' and mKO '3' based on their blue cover-scale phenotypes: mKO 'A' exhibited large blue mutant patches, whereas mKO '3' showed comparatively smaller blue patches (electronic supplementary material, figure S2). We also selected mKO 'M' for its asymmetrically disrupted eyespot phenotype (electronic supplementary material, figure S5). Because we cannot

reliably obtain sufficient DNA from small patches of adult wing scales, we extracted DNA (Omega Bio-Tek, Norcross, GA, USA) from the thoracic flight muscles. As these are G0 mosaics, somatic editing can differ among tissues. Thus, thoracic genotypes confirm that editing occurred in each individual but may not fully capture the indel composition of wing-scale cell lineages underlying any given patch of wing scales—a limitation inherent to tissue-based genotyping of CRISPR mosaic wings. We used polymerase chain reaction (PCR) to amplify DNA from around the potential cut sites using the primers 5′-ATACTAAACCCTGCACCCGC-3′ and 5′-ACGTACTCACAAGCGAACGT-3′. We ran amplified DNA from wild-type and mutant individuals on an agarose gel and purified (Monarch DNA Extraction and Purification kit, New England Biolabs, MA, USA) and cloned the PCR products into JM109 competent cells using pGEM®-T Easy Vector Systems (Promega Corporation, Madison, WI, USA). Transformed cells were amplified and Sanger sequenced at the Genomics Facility, Cornell Institute of Biotechnology, Ithaca, NY, USA.

(d) Micro-spectrophotometry of wing scales

We mounted individual wing scales (n = 3) from wild-type and *araucan* mutant *J. coenia* butterflies on glass slides and measured their normal-incidence reflectance spectra using a mercury-xenon light source (Thorlabs, NJ, USA) connected to a uSight-2000-Ni micro-spectrophotometer (Technospex Pte. Ltd., Singapore). We used a Nikon TU Plan Fluor 100× objective (numerical aperture = 0.9) to collect spectra and calibrated the set-up with a dielectric mirror. For each measurement, we averaged 10 scans with an integration time of 100 ms. We recorded three measurements from different locations on each of three scales per genotype and averaged them to obtain a representative reflectance spectrum. While these measurements do not provide a goniometric quantification of viewing-angle dependence, visual inspection of mutant scales revealed angle dependency of colour and a shimmering effect consistent with *J. coenia* iridescence as previously described [2,3].

To measure absorbance, we used the same optical set-up with a 20× objective (NA = 0.5). We mounted individual scales (n = 5) submerged in clove oil (Hayashi Pure Chemical Ind., Ltd.) between a slide and coverslip to match the refractive index of chitin and used a clove oil-covered transparent area of the slide as a reference. For each genotype, we measured three locations on each of five scales and averaged the data to generate absorbance spectra.

We performed all spectral analysis and visualization using the pavo 2 package in R [20]. To test for significant differences in spectral values between wild-type and *araucan* mutant scales, we conducted independent two-sample t-tests at each 50 nm increment from 350 to 700 nm. We applied the Benjamini–Hochberg false discovery rate method to adjust p-values for multiple comparisons and considered adjusted p-values < 0.05 as significant.

(e) Scanning electron microscope imaging of wing scales

We used scanning electron microscopy (SEM) to assess structural differences between wild-type and *araucan* mutant scales. We mounted individual scales (n = 5) from mutant mosaic clones and contrasting wild-type regions on carbon tape and sputter-coated them with platinum (JEOL JFC-1600) for 30 s at 30 mA. We imaged the samples using a FEI Versa 3D with the following parameters: voltage 10 kV, current 32 pA. To obtain transverse sections of wing scales, we used focused ion beam (FIB) milling with the gallium ion beam of the FEI Versa 3D, applying a beam voltage of 8 kV, a beam current of 25 pA and a tilt of 52°. We performed the FIB-SEM in the Electron Microscopy Facility, National University of Singapore.

We obtained the transverse section of the scales shown in figure 1c by cryo-fracturing the scales following a previously described protocol [21]. We then mounted whole and cryo-fractured scales of interest on carbon tape and sputter-coated them with an 8 nm layer of gold using a Cressington 208 HR Sputter Coater. We acquired the image on an FEI Teneo LV SEM using the Everhard Thornley detector and beam parameters of 5.00 kV 6.3 pA with a 10 µs dwell time. We used cryo-fracturing only to generate the image used in figure 1c. All measurements for laminar thickness reported were done on scales that were milled using FIB and imaged using SEM.

(f) Measurement of scale ultrastructure and statistical analysis

We quantified scale ultrastructure by measuring three parameters: lower lamina thickness (LL), inter-ridge distance (d_{RR}) and cross-rib ($d_{CR\text{-}CR}$) spacing (figure 1c,d). We performed all measurements in Fiji using the line tool [22]. For FIB milling, the sample block face was tilted to a 52°, corresponding to the fixed geometry between the SEM and the gallium ion columns in our dual-beam instrument, so the ion beam could mill a trench and expose a transverse cross-section on the scale. Because SEM images of the milled cross-sections were acquired at this tilt (i.e. not viewed in a top-down 90° orientation), the apparent LL measured in the image is a foreshortened projection of the true thickness. We, therefore, corrected LL by dividing the measured value by sin 52° (corrected LL = measured thickness/sin 52°) following a standard geometric correction described previously [23]. We collected measurements from cover scales in the dorsal non-eyespot region, and from cover and ground scales from the eyespot centre. For each wing location and genotype, we analysed five individual scales sampled across two biological replicates. Within each scale, we quantified ultrastructure by taking independent measurements at distinct positions (LL: 10 measurements per scale; inter-ridge distance: 25 per scale; cross-rib spacing: 50 per scale) to capture within-scale variation.

We analysed scale ultrastructure data using linear mixed-effects (LME) models implemented in the R package nlme v. 3.1 [24], which accounts for hierarchical data structures. For each geometric parameter (LL, inter-ridge distance and cross-rib spacing), we treated scale type as a fixed effect and included scale identity nested within individual butterfly as a random effect. To address heteroscedasticity among scale types, we applied the varIdent() function. We selected the best-fitting model

based on the Akaike information criterion (AIC). We conducted pairwise comparisons of group means using the multcomp R package. We report *p*-values and 95% confidence intervals for all pairwise comparisons in tables 1 and 2. A summary of the fixed effects from the LME models, including degrees of freedom, *F*-values and *p*-values, is provided in the electronic supplementary material, tables S3 and S4. Raw measurement data are also included to support independent reanalysis (see the Data accessibility section).

(g) Hybridization chain reaction fluorescent *in situ* hybridization of *araucan*

We designed a hybridization chain reaction (HCR) probe set targeting the coding sequence of *araucan* in *J. coenia* using 19 pairs of 25 bp probes (50 bp per site) spanning the annotated transcript (electronic supplementary material, file S2). We ordered the probes as oligonucleotides from Genewiz (Azenta Life Sciences, Morrisville, NC). We confirmed probe specificity by BLAST searching against the most recent *J. coenia* genome assembly, ensuring no off-target binding sites.

For HCR experiments, we dissected last instar larval imaginal discs, as well as pupal wings at 13% (first day post-pupation), 25% (second day post-pupation) and 45% (third day post-pupation) of pupal development (PD). We used *araucan* probes paired with B1 initiators and visualized them with Alexa Fluor 647-labelled hairpins. As a positive control, we used *spalt* probes labelled with B3 initiators (electronic supplementary material, file S2) and visualized them in the 546 nm channel. For the electronic supplementary material, figure S7, we performed HCR of *optix* with B5 initiator (electronic supplementary material, file S2). We performed co-detection of *araucan* and *spalt* expression in wings from one side of each individual, while using the contralateral wings as negative controls. In these controls, we omitted the probes but followed all other HCR steps to assess background fluorescence. We performed the HCR following the protocol described by Bruce *et al.* (dx.doi.org/10.17504/protocols.io.bunznvf6). To capture pattern-specific expressions across the entire wing tissue, we used a Keyence BZ-X800 fluorescence microscope in the laboratory of Dr Anyi Mazo-Vargas (Department of Biological Sciences, Duke University).

3. Results

(a) *araucan* knockouts result in iridescent blue scales via laminar thickening

We injected 758 eggs with Cas9 and *araucan* sgRNAs, of which 179 hatched and 117 survived to adulthood. Twenty-two of the adults that emerged had mutant wing colour phenotypes. We observed two distinct classes of mutations, both of which involved iridescent colouration: (i) blue iridescence in mutant clones across the dorsal wing surface ($n = 13$); and (ii) a shift from purple-violet to grey-brown specifically in eyespot centres ($n = 9$). These two phenotypic classes were mutually exclusive, and no individuals displayed both dorsal blue clones and disrupted eyespot centre colouration. Detailed descriptions and numbers of individuals representing each mutant phenotypic class are summarized in the electronic supplementary material, table S1. We genotyped representative mutants from each class (dorsal blue: mKO 'A' and mKO '3', electronic supplementary material, figure S2; eyespot centre: mKO 'M', electronic supplementary material, figure S5) to verify mutagenesis and confirmed deletions at the sgRNA target sites in the *araucan* coding region (electronic supplementary material, figure S1c). Because these are G0 mosaics and genotyping does not resolve the spatial distribution of edited cell lineages within each wing, we treat haplotype recovery as confirmation of editing rather than evidence that particular deletion haplotypes underlie the distinct phenotypic classes.

The 13 individuals that showed mosaic clones of blue iridescence showed the phenotype exclusively on dorsal wing surfaces (figure 1a; hindwings: electronic supplementary material, figure S2; forewings: electronic supplementary material, figure S3 and table S1). Since iridescent blue-coloured scales can be artificially selected for in populations of *J. coenia* [3], we assessed individuals from our wild-type colony for similar iridescent scales to rule out the possibility of phenotypes being because of natural variation. Out of the individuals randomly observed ($n = 32$), we did not observe any blue iridescent scales on the dorsal surface of the hindwings, which supports that the blue iridescence in the mKOs is a result of knockout of *araucan* (chi-squared test, $p < 0.005$). This conclusion was also supported by the fact that individuals with iridescent patches of scales presented this phenotype asymmetrically (electronic supplementary material, figures S2 and S3), consistent with cell lineage mosaicism [2], whereas natural variation in iridescence is typically symmetrical. In addition, within visually defined dorsal mutant patches, the blue phenotype was frequently expressed in a peppered manner at the single-scale level—vivid blue cover scales were interspersed among scales that retained wild-type colouration (figure 1a; electronic supplementary material, figures S2–S4). This scattered penetrance contrasts with the more uniformly transformed clonal patches often reported for other butterfly G0 CRISPR mosaics and indicates that a contiguous patch does not necessarily correspond to a uniform functional knockout state across all scale cells. Because our G0 mosaics show a scattered peppering penetrance at the single-scale level and dorsal ground scales lack a clear diagnostic visible phenotype (electronic supplementary material, figure S4), we could not unambiguously classify individual dorsal ground scales as mutant versus wild-type for quantitative comparison. Moreover, the visible blue shift in dorsal mutant patches is confined to the cover-scale layer, consistent with prior work in *Junonia* showing that variation in cover-scale LL strongly predicts the brown-to-blue/green spectrum of structural colour [3]. We, therefore, focused our optical and ultrastructural analyses on dorsal cover scales.

The shift from golden-brown cover scales in the wild-type to vivid blue in mutants was quantified using reflectance spectrophotometry. Mutant scales exhibited increased reflectance in the ultraviolet and blue wavelengths (<500 nm), while wild-type scales reflected more light in longer wavelengths (>500 nm), consistent with their golden-brown appearance (figure 1b). To determine whether this observed colour change was structural or pigmentary in origin, we immersed individual scales

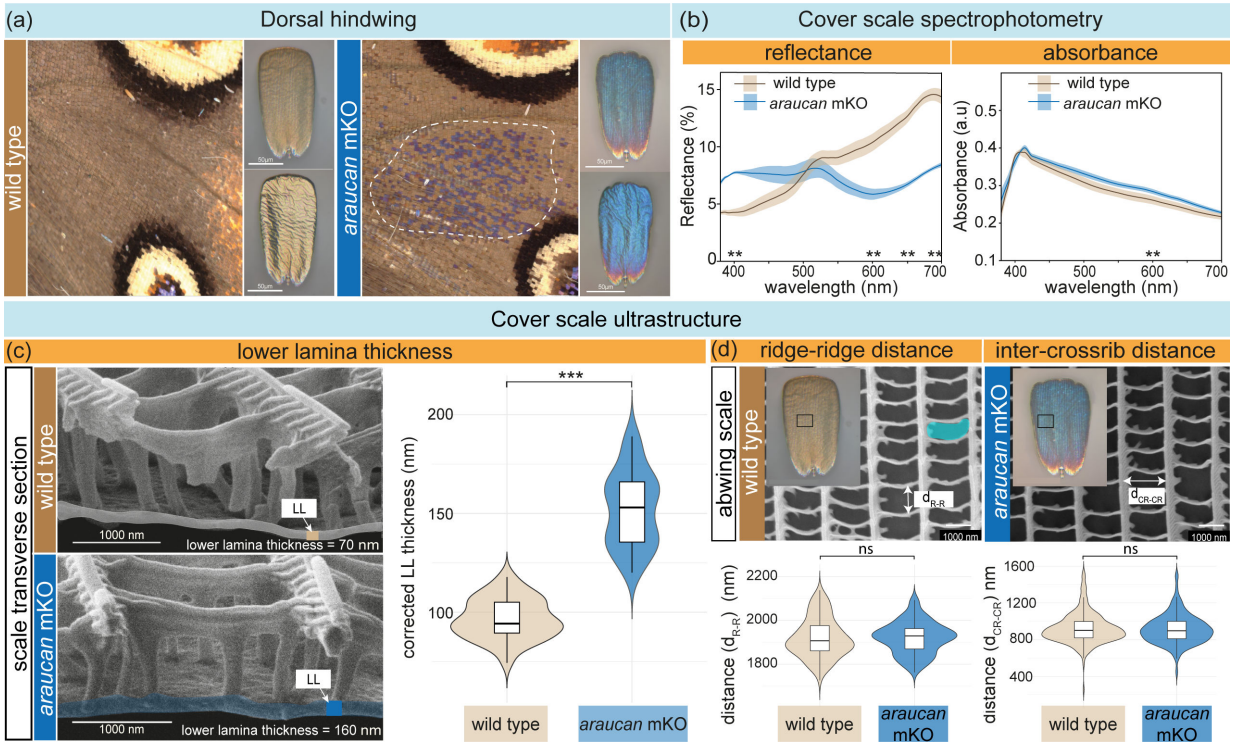

Figure 1. *araucan* knockouts cause blue iridescence in dorsal hindwings by increasing lower lamina thickness (LL) of cover scales. (a) *araucan* mKO produces patches of blue iridescent scales in the dorsal hindwing. Left: wild-type wing showing uniform golden-brown colour. Adjacent are magnified views of individual cover scales from the same wing, with the abaxial surface (top) and adaxial surface (bottom) shown. Right: *araucan* mKO hindwing showing a mosaic patch of blue iridescent scales (dashed line). Adjacent are magnified views of mutant cover scales, revealing blue iridescence on both the abaxial (top) and adaxial (bottom) surfaces. Scale bar = 50 µm. Additional images of contralateral wings showing mutant blue iridescent scales are in the electronic supplementary material, figures S2 and S3. (b) Reflectance and absorbance spectra of cover scales confirm that the observed colour shift is structural, not pigment-based. Solid lines indicate mean spectra; shaded regions represent standard deviation; asterisks mark wavelengths with significant differences between groups ($n_{reflectance} = 3$; $n_{absorbance} = 5$; $^{**}p_{adj} < 0.01$; electronic supplementary material, table S3). (c) Left: SEM images of transverse sections from isolated cover scales, prepared by cryo-fracturing, show that wild-type scales (top) have a thinner lower lamina (LL; grey shaded region) compared to mutant scales (bottom; blue shaded region). Right: violin-box plot quantifies LL from FIB-milled isolated cover scales ($n = 5$; $^{***}p < 2 \times 10^{-16}$; table 1; electronic supplementary material, table S2). (d) Additional cover scale measurements: ridge-to-ridge spacing (d_{R-R}, top left), distance between crossribs (d_{CR-CR}, top right), and area of the windows (teal)—through which incident light goes into the scale (bottom, n.s.—not significant; table 1; electronic supplementary material, table S2).

Table 1. Comparison of wild-type (WT) and *araucan* mutant non-eyespot cover scale ultrastructural features. (*** $p < 0.001$; CI, confidence interval.)

scale type	factor	comparison	estimate	std error	*Z*-value	Pr(>|*z*|)	95% CI
cover	lower lamina thickness	WT − mutant = 0	−55.41	2.93	−18.89	$<2 \times 10^{-16}$ ***	[−61.16; −49.66]
cover	distance ridge–ridge	WT − mutant = 0	0.54	0.54	10.13	0.05	[−19.32; 20.39]
cover	distance crossrib–crossrib	WT − mutant = 0	8.61	14.25	0.6	0.54	[−19.31; 36.54]

in oil, which matches the refractive index of chitin and thereby suppresses structural colouration. As in previous studies, absorbance spectra collected under these refractive index-matched conditions provide a measure of the light transmitted through the scale and served as a proxy for pigment content, as differences in pigment type and concentration result in distinct patterns of wavelength-specific light absorption [3,7,21,25–28]. We observed minimal differences in absorbance of visible wavelengths between mutant and wild-type scales (figure 1b; electronic supplementary material, table S3), indicating that the shift in colouration is primarily owing to structural changes rather than differences in pigmentation.

To investigate the ultrastructural basis of the iridescent blue colouration in *araucan* mutant scales, we measured the thickness of the lower lamina—a key structural determinant of scale colour in butterflies of the *Junonia* genus, where a thicker lower lamina causes a shift towards bluer hues [3]. We quantified laminar thickness in both wild-type brown scales and blue mutant scales to assess whether this relationship held true in our *araucan* knockouts. SEM imaging after FIB milling to get the transverse section of scales revealed that mutant cover scales had significantly thicker lower laminae compared to wild-type (figure 1c; LME model, AIC-selected best fit, $p < 2 \times 10^{-16}$; table 1; electronic supplementary material, table S2). The mean corrected LL in wild-type scales was 96.7 ± 10.2 nm, while mutant scales averaged 152.0 ± 18.9 nm, supporting the hypothesis that the observed colour shift is structurally mediated.

To assess whether additional ultrastructural features contribute to the iridescent colour shift observed in *araucan* mutants, we quantified ridge spacing and cross-rib distances in cover scales. These geometric features determine the size of the scale

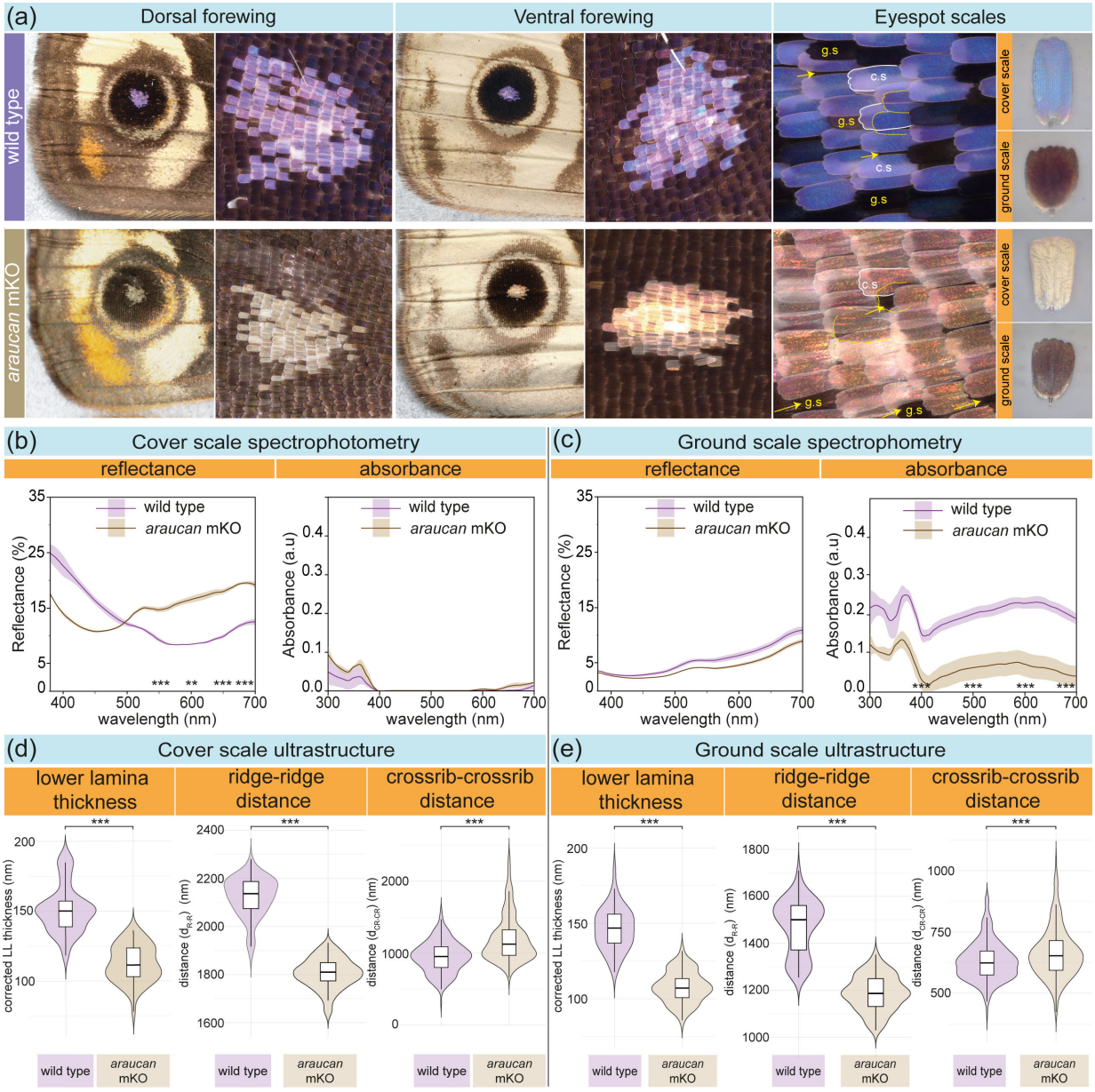

Figure 2. *araucan* knockouts diminish purple-violet iridescence by altering cover scale reflectance, ground scale pigmentation, and the ultrastructure of both scale types in forewing eyespot centres. (a) On both dorsal (left) and ventral (middle) surfaces, forewing eyespot centres of wild-type individuals (top) exhibit distinct purple-violet iridescence, whereas *araucan* knockouts (bottom) show muted grey-brown scales (electronic supplementary material, figure S5). Magnified images of the eyespot centre (right) highlight the stacking arrangement of cover scales (c.s; white border) and ground scales (g.s; yellow arrows where exposed and yellow dashed boundaries where overlaid by cover scales). Overlaid ground scales highlight saturation of overall colour (yellow dashed boundary). Abwing surfaces of isolated cover and ground scales (far right) of wild-type (top) and mutant (bottom) scales. (b) Spectrophotometry of isolated cover scales and (c) ground scales from eyespot centres in wild-type and mutant forewings. Reflectance spectra (left) and absorbance spectra (right). Solid lines represent mean spectra; shaded areas indicate standard deviation; asterisks denote wavelengths with significant differences between groups ($n_{reflectance} = 3$; $n_{absorbance} = 5$; ***p-$_{adj} < 0.001$, **p-$_{adj} < 0.01$; electronic supplementary material, table S5). (d,e) Violin-box plots quantifying ultrastructural features in cover scales (d) and ground scales (e) ($n = 5$; ***$p < 2 \times 10^{-16}$; table 2; electronic supplementary material, table S4).

Table 2. Comparison of wild-type (WT) and *araucan* mutant cover and ground scale ultrastructural features collected from eyespot centre. (*** $p < 0.001$; CI, confidence interval.)

scale type	factor	comparison	estimate	std error	*Z*-value	Pr(>|*z*|)	95% CI
cover	lower lamina thickness	WT − mutant= 0	38.92	2.61	14.89	$<2 \times 10^{-16}$ ***	[33.79; 44.04]
cover	distance ridge−ridge	WT − mutant = 0	317.75	6.83	46.51	$<2 \times 10^{-16}$ ***	[304.36; 331.14]
cover	distance crossrib−crossrib	WT − mutant = 0	−256.73	24.15	−10.63	$<2 \times 10^{-16}$ ***	[−304.06; −209.40]
ground	lower lamina thickness	*p*	38.46	2.45	15.72	$<2 \times 10^{-16}$ ***	[33.67; 43.25]
ground	distance ridge−ridge	WT − mutant = 0	282.4	6.87	41.08	$<2 \times 10^{-16}$ ***	[268.93; 295.88]
ground	distance crossrib−crossrib	WT − mutant = 0	−32.52	7.49	−4.34	1.42×10^{-5} ***	[−47.20; −17.83]

'windows' that determine the amount of incident light that interacts with underlying scale nanostructures (figure 1d). Mean ridge-to-ridge spacing was comparable between wild-type brown and mutant blue scales (wild-type: 1921 ± 90 nm; mutant: 1921 ± 73 nm; figure 1d; table 1; electronic supplementary material, table S2), and cross-rib distance was also unchanged (wild-type: 923 ± 167 nm; mutant: 914 ± 160 nm; figure 1d; table 1; electronic supplementary material, table S2). Thus, the colour shift is unlikely to be explained by changes in ridge or cross-rib spacing and is most consistent with increased LL and a thin-film interference mechanism, as supported by prior work in this species [3]. However, because we did not quantify other ultrastructural parameters such as ridge height or ridge lamellar layering (which can form multilayer reflectors in some butterflies) [29,30], we cannot fully exclude additional contributions from these features.

(b) *araucan* knockouts eliminate purple-violet iridescence in forewing eyespot centres

Nine of the recovered *araucan* mKOs exhibited a striking phenotype affecting the scales in the forewing eyespot centres. In wild-type *J. coenia*, these eyespot centres exhibit a vivid purple-violet iridescence (figure 2a; electronic supplementary material, figure S5). By contrast, *araucan* mutants lacked this strong purple-violet colouration, which was replaced by a muted grey-brown hue, occasionally with faint traces of pink or violet iridescence (figure 2a; electronic supplementary material, S5). The loss of purple-violet iridescence was asymmetrical in all but two individuals (electronic supplementary material, figure S5), validating the mosaic nature of the knockout phenotype. Notably, eyespot centres on the hindwings were unaffected.

The iridescent purple-violet colouration of *J. coenia* eyespot centres arises from the combined optical properties of both cover scales and underlying ground scales. The ground scales enhance the overall saturation of the reflected colour when stacked beneath the more translucent cover scales (highlighted by yellow dashed outlines in figure 2a). Because this mechanism is consistent with observations in other butterfly species exhibiting purple-violet colouration [31,32], we characterized the optical properties of each scale type within the eyespot centre. Specifically, we measured reflectance spectra and refractive index-matched absorbance spectra of both cover and ground scales in the forewing eyespot centre to identify which scale type and optical mechanism was contributing to the observed colour shift.

Spectral analysis showed that both scale types, cover and ground, were altered in the *araucan* mutants differently, resulting in the observed colour shift. Mutant cover scales exhibited increased reflectance above 500 nm, corresponding to a duller grey-brown colouration, whereas wild-type cover scales reflected more light in the ultraviolet to violet wavelengths (380–450 nm), producing the observed purple-violet hue (figure 2a,b). By contrast, reflectance measurements of ground scales revealed no significant differences between wild-type and mutant individuals (figure 2c). To assess pigment contributions independent of structural effects, we measured absorbance in a refractive index-matched medium. Under these conditions, both wild-type and mutant cover scales showed minimal light absorption in the ultraviolet and red regions, with no significant differences between groups, indicating that most incident light was transmitted through the cover scales (figure 2b). However, mutant ground scales showed a different pattern across the ultraviolet and visible spectrum (300–700 nm) where they exhibited significantly lower absorbance compared with wild-type scales, suggesting reduced light-absorbing pigmentation in the mutants (figure 2c).

To identify structural components in the scales that might have been altered, we characterized lamina thickness, ridge spacing and cross-rib distances in both cover and ground scales. We found that the lower lamina was significantly thicker in the eyespot scales of wild-type individuals compared to *araucan* mutants in both scale types. In cover scales, the LL averaged 151 ± 16.9 nm in wild-types and 112 ± 13.1 nm in the mutants (LME model, AIC-selected best fit, $p < 2 \times 10^{-16}$; figure 2d; table 2; electronic supplementary material, table S4). A similar pattern was observed in ground scales (146 ± 13.9 nm in wild-types versus 108 ± 10.3 nm in mutants, $p < 2 \times 10^{-16}$; figure 2e; table 2; electronic supplementary material, table S4).

Ridge spacing was significantly narrower in mutants versus wild-type scales, for both scale types. In cover scales, ridge spacing was 2123 ± 82.9 nm in wild-types and 1805 ± 62.9 nm in mutants ($p < 2 \times 10^{-16}$; figure 2d; table 2; electronic supplementary material, table S4), and in ground scales, 1470 ± 116 nm in wild-types versus 1188 ± 74 in mutants ($p < 2 \times 10^{-16}$ figure 2e; table 2; electronic supplementary material, table S4). By contrast, the distance between crossribs was significantly greater in *araucan* mutants for both scale types. In cover scales, mutants had crossrib spacing of 1202 ± 322 nm compared with 946 ± 217 in wild- types ($p < 2 \times 10^{-16}$; figure 2d; figure 2; electronic supplementary material, table S4); and in ground scales, mutants had 663 ± 103 nm of spacing versus 631 ± 79.3 nm in wild-types ($p = 1.42 \times 10^{-5}$; figure 2e; table 2; electronic supplementary material, figure S4). Together, these optical and structural analyses reveal that *araucan* knockouts disrupt the pigmentation of ground scales and the nanostructural organization of both cover and ground scales in the eyespot centres. In combination, these changes probably underlie the loss of saturated purple-violet iridescence and its replacement with muted hues in *araucan* mutants.

(c) Dynamic spatial and temporal expression of *araucan* in the developing wing

Our mKOs demonstrate that *araucan* is necessary for normal structural colouration of *J. coenia* wing scales and appears to play a role in determining scale structure itself. Accordingly, we hypothesized that we should observe *araucan* expression in wings during scale morphogenesis. Because *Iroquois*-complex genes—including *araucan*—exhibit pattern-specific expression in the *D. melanogaster* wing disc [12,13], we further sought to ask whether *araucan* is expressed in a pattern-specific manner in the developing *J. coenia* wings, including in regions affected in mutants (e.g. eyespot centres), or in other defined wing domains across development. To characterize spatial transcriptomic patterns, we performed HCR *in situ* hybridization for *araucan* messenger RNA at key developmental stages: (i) in last-instar wing discs, immediately during and after the transcription factor

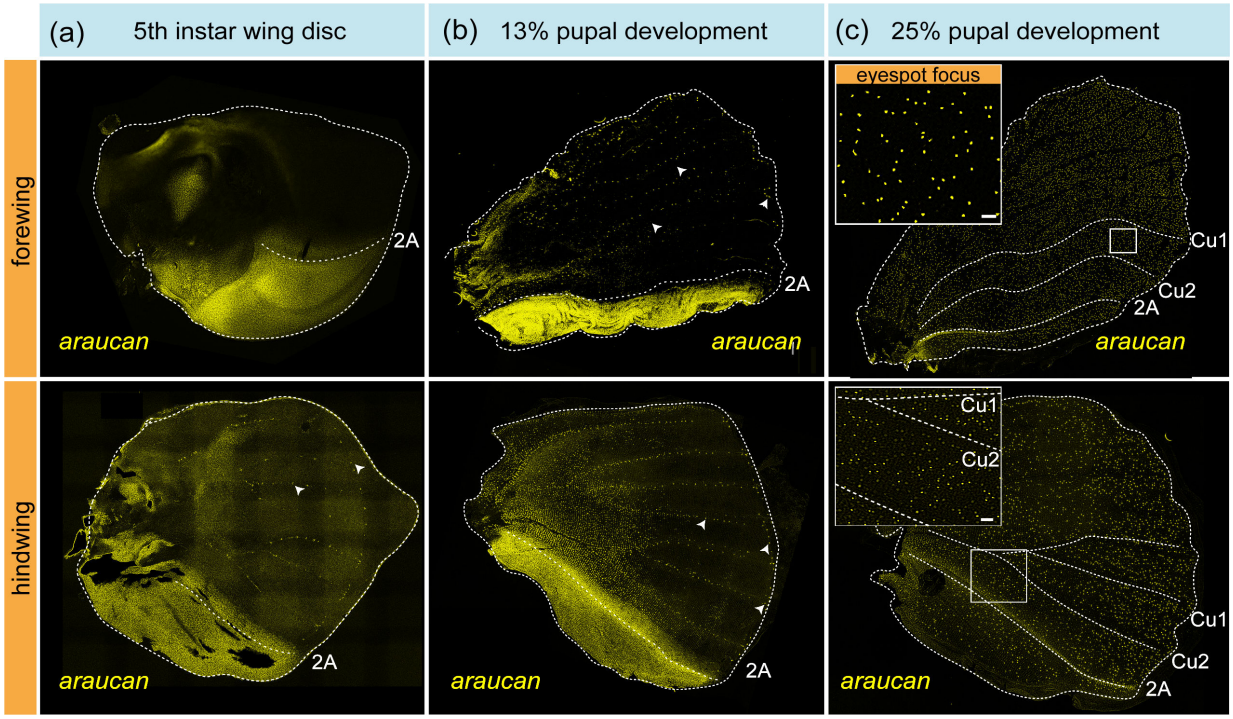

Figure 3. Spatiotemporal dynamics of *araucan* transcripts in late larval and early pupal wings**.** (a,b) In the fifth-instar larva (a) and approximately 13% pupal development (PD) (b), *araucan* signal (yellow) is enriched in the far-posterior vannus domain, bounded anteriorly by the 2A vein in both wings. Signal is also detected in cells along pre-vein tracheae and at the wing margin (white arrows). (c) By approximately 25% PD, *araucan* persists along the 2A vein and appears in scattered cells across the wing blade in a pattern-nonspecific manner (yellow dots). In the forewing (top), this includes the eyespot focus (inset). In the hindwing, this recaptures the mosaic clones seen in the mKOs (inset). Scale bar = 50 µm.

Spalt defines future eyespot domains [33–35]; and (ii) in pupal wings at two time points 13% PD, when eyespot centres have been established, and 25% PD, when scale precursors differentiate into scale cells [36].

In last-instar wing discs, *araucan* transcripts are enriched in the posterior wing domain (vannus) bounded by the 2A vein (figure 3a). An additional signal appears in an anterior–proximal region and in enlarged cells arrayed along the trachea that mark future veins and the wing margin (figure 3a; electronic supplementary material, figure S6b). At approximately 13% PD, the posterior-domain expression persists, and *araucan* is detected in large cells interspersed along the veins of both forewings and hindwings (figure 3b). By approximately 25% PD, posterior-domain signal contracts to a narrow stripe flanking the 2A vein, while expression becomes broadly peppered across both wings without aligning to obvious adult colour elements (figure 3c). This expression, along with the expression in the veins, persists into later PD (electronic supplementary material, figure S6e). Across stages co-stained with the eyespot marker *spalt*, we did not detect *araucan* expression obviously upregulated in eyespots (electronic supplementary material, figure S6), despite peppered expression spanning those regions in the stages sampled after 13% PD (figure 3c).

Together, these data show that *araucan* transitions from early domain- and vein-associated patterns to a later dispersed distribution in developing scale cells. This later peppered expression provides a plausible explanation for the scattered blue-scale phenotypes in mosaic mutants where, within a broader territory, only the subset of scale cells that would normally deploy *araucan* at the relevant stage would be expected to show a structural-colour shift when *araucan* function is lost.

4. Discussion

(a) Region-specific control of iridescence by *araucan*

In this study, we investigated the role of the *Iroquois*-complex gene *araucan* in butterfly wing patterning. Our findings reveal that *araucan* is a key regulator of structural colouration in *J. coenia*, modulating iridescence in two spatially and functionally distinct ways: (i) by suppressing blue iridescence across the dorsal wing surface; and (ii) by promoting purple-violet iridescence in forewing eyespot centre.

Structural colouration in butterfly wings arises from complex interactions between incident light and the ultrastructure of wing scales, as reviewed by Thayer & Patel [37]. One well-characterized mechanism is thin-film interference, in which the lower lamina of the scale functions as a reflective surface, producing a range of iridescent hues depending on its thickness and the angle of incident light [31,37–39]. Previous work in *Junonia* spp. has shown that the thickness of the lower lamina within individual cover scales reliably predicts spectral reflectance: thin laminae generate golden-brown hues as seen in wild-type *J. coenia*, whereas thicker laminae produce blue or teal hues as seen in *optix* knockouts of *J. coenia* or species in the genus that naturally exhibit blue-green iridescence [3]. In our *araucan* knockouts, we observed an increase in LL in dorsal cover scales, resulting in a shift from brown to blue structural colouration. Because we detected no pigmentation changes, the

dorsal brown-to-blue shift is best explained by increased cover-scale LL, indicating that *araucan* normally constrains laminar thickening in dorsal cover scales.

A striking feature of *araucan* mosaics is the dorsal 'peppering' of blue scales interspersed among apparently wild-type scales. Our HCR data suggest a plausible explanation: *araucan* transcripts become broadly scattered around the scale differentiation window (approx. 25% PD), implying that *araucan*-dependent regulation of laminar thickening may be deployed heterogeneously across developing scale cells. Under this model, even if a contiguous edited territory shared a common knockout genotype, it would not necessarily yield a uniform phenotype—only cells that normally express *araucan* above a functional threshold during the scale maturation window would be expected to thicken the lower lamina and shift to blue when *araucan* is lost. Cell-to-cell variation typical of G0 mosaics (e.g. monoallelic versus biallelic loss-of-function) could further accentuate this heterogeneity. Dorsal ground scales show no obvious visible phenotype (electronic supplementary material, figure S4), but subtler effects lacking a diagnostic colour readout remain possible. Distinguishing among these possibilities will require direct ultrastructural quantification and scale-cell-resolved expression and genotyping in stable mutant lines.

In contrast to the dorsal blue scales, the eyespot centres of wild-type *J. coenia* display purple-violet iridescence that emerges from the combined optical effects of stacked cover and ground scales as shown in other nymphalid butterflies [31,32,38]. The ultrastructure and pigmentation of the cover scales modulate the amount of incident light reflected or transmitted, while those of the underlying ground scales influence the extent of light that is scattered back. Together, these layers generate interference patterns that either enhance or dampen the resulting colour signal. In *araucan* mutants, we observed decreased laminar thickness in both cover and ground scales, accompanied by a marked reduction in ground-scale pigmentation. We infer that the loss of pigment decreases light absorbance, thereby increasing backscatter, which—when combined with structural modifications in the cover scales—produces a desaturated, muted tan-grey hue in place of the saturated purple-violet seen in wild-type eyespots. This enhanced backscatter probably contributes to the shimmering or hazy appearance of iridescence observed in some mutant individuals (electronic supplementary material, figure S5). In addition, differences in ridge spacing and cross-rib distances may further influence optical properties, either directly or indirectly through effects on pigmentation [27]. Together, these results demonstrate that *araucan* regulates multiple dimensions of scale morphology and pigmentation that collectively shape the optical characteristics of forewing eyespot centre colouration.

The opposing effects of *araucan* in eyespot versus non-eyespot scales underscore a broader principle in butterfly wing development: regulatory genes often function in a region-specific, context-dependent manner. This contrast—structure-only effect outside of the eyespots versus coupled structural and pigmentary disruption in eyespot centres—suggests that *araucan* acts within distinct regulatory environments in these regions. One possibility is that eyespot-specific regulators (e.g. *spalt*, *distal-less*) [38] provide the necessary regulatory landscape that redirects *araucan* towards pigment-related targets in eyespot centres, whereas outside the eyespots its primary output is laminar thickening. Alternatively, pigmentation loss in the eyespots could be an indirect consequence of altered scale morphogenesis, coupling structural and pigmentary changes in the eyespot scale cells. The divergent roles of *araucan* reinforce the idea that eyespots represent modular, semi-independent developmental units capable of evolving specialized scale properties—including iridescence—without altering patterning in adjacent regions. This spatial modularity enables flexible evolutionary innovation within the wing, raising important questions about the regulatory architecture controlling *araucan* expression across the wing.

(b) Gene regulatory dynamics of *araucan*

We were intrigued to observe that *araucan* had a very dynamic pattern of transcription over developmental time, ranging from vein- and posterior domain-related patterns in early development to a whole-wing scattered pattern later in PD that is consistent with iridescence phenotypes. The early posterior domain expression pattern was of particular interest because it resembles the expression of *mirror*–the sister gene of *araucan,* which has been shown to play a role in posterior domain determination [11]. Curiously, we did not observe any domain-related or otherwise *mirror*-like phenotypes in our *araucan* mutants, and it therefore remains unclear whether this posterior *araucan* expression pattern has any functional relevance. It is interesting, however, to speculate whether the parallel expression patterns of *araucan* and *mirror* may reflect ancestral regulatory architecture that predates the divergence of these genes. In any case, the complex and dynamic expression patterns of *araucan* over developmental time suggest this gene is probably responding to a varied progression of upstream trans-regulatory signals.

Our CRISPR mKOs and expression data raise the question of where *araucan* sits within the gene regulatory networks that pattern the wing and specify scale-cell fates. One of the two major mKO classes we observe is a blue shift in the iridescence of dorsal wing scales, consistent with increased LL in cover scales. A very similar effect was previously reported for *optix* mKOs in *J. coenia* [2], suggesting that these perturbations converge on a shared phenotypic output. However, we currently lack the cell-type and stage-matched expression data and functional epistasis experiments needed to infer whether *optix* and *araucan* act in a linear hierarchy or as largely independent inputs that converge on common downstream effectors. Although we did not detect marked co-expression of *optix* and *araucan* at the time points sampled (electronic supplementary material, figure S7), this does not rule out coordination at later stages of scale maturation, transient or low-abundance co-expression, or non-cell-autonomous interactions. We, therefore, outline two working models: (i) a shared-pathway model in which *optix* and *araucan* act in series and/or within a common regulatory module that influences lower lamina thickening, such that loss of either gene can shift LL; or (ii) a parallel-input model in which *optix* and *araucan* act largely independently but converge on overlapping 'effector' programmes that tune LL and generate similar blue-shift phenotypes. In either case, the most conservative mechanistic link between transcriptional regulation and lamina thickness is through modulation of late-scale maturation processes such as the timing and extent of cuticle/chitin deposition and matrix assembly, secretion/trafficking of cuticular components and/or

cytoskeletal organization that shapes scale-cell architecture and morphogenesis. Distinguishing between these models and identifying the most relevant downstream processes will require stage-specific expression sampling and explicit tests of genetic interaction (e.g. double perturbations or staged knockdowns).

In addition to structural blue shifting of dorsal wing scales, *araucan* had a different, yet highly specific effect on the structural and pigmentary colouration of eyespot centres. How might *araucan* be deployed for such a different, spatially restricted eyespot function? In *J. coenia*, mKO of *spalt* eliminates all eyespots [40], consistent with *spalt* acting as a master regulator of eyespot formation. Because the *araucan* eyespot phenotype tracks *spalt* expression territories, one plausible model is that eyespot gene regulatory networks inputs (potentially including *spalt*) place *araucan* or its functional activity under eyespot-specific control. The absence of detectable *spalt–araucan* co-expression in our HCR *in situ* does not rule out that *araucan* transcription in eyespot cells may fall below our detection threshold and/or occur at later stages of wing development, consistent with a role in terminal stages of scale maturation. A similar detection-phenotype mismatch is familiar from other wing transcription factors (e.g. *optix*), where early *in situ* patterns (electronic supplementary material, figure S7) can contrast with broader or later phenotypic effects of perturbation. An alternative, non-mutually exclusive possibility is that *araucan* is expressed broadly at low levels, but its eyespot-specific impact is gated by spatially restricted (*cis-* and/or *trans-*) regulatory elements established by the eyespot regulatory network. Together, these points suggest that low threshold and late-stage specific gene activity, despite being technically challenging to capture, may be particularly important for structural and pigmentary colour determination [2]. The forewing-specific *araucan* eyespot phenotype also leads us to speculate that *Ultrabithorax*, a selector gene for hindwing identity [41–44], may play an upstream role in regulating *araucan* in this context.

5. Conclusion

Overall, our results identify *araucan* as a region-specific regulator of structural colouration in *J. coenia*, suppressing blue iridescence across the dorsal wing while promoting saturated purple-violet at the forewing eyespot focus. These effects map to coordinated changes in scale ultrastructure—especially LL—and, in eyespots, to coupled shifts in optical layering with ground-scale pigmentation. Together, the data reveal how a single transcription factor can differentially tune photonic architecture across the wing and reinforce eyespots as modular, context-dependent developmental units. While the precise placement of *araucan* within colour pattern gene regulatory networks remains unresolved, our findings establish a framework for dissecting the regulatory logic that links gene activity to the coordinated evolution of cell structure and pigment synthesis.

Ethics. This work did not require ethical approval from a human subject or animal welfare committee.

Data accessibility. The raw SEM images used for ultrastructural measurements, associated data tables of scale ultrastructure, and raw spectral data from scale micro-spectrophotometry are available through Dryad [45].

Supplementary material is available online [46].

Declaration of AI use. We have not used AI-assisted technologies in creating this article.

Authors' contributions. M.C.: conceptualization, data curation, formal analysis, investigation, methodology, project administration, supervision, visualization, writing—original draft; C.F.: data curation, formal analysis, investigation, methodology, validation, visualization, writing—original draft, writing—review and editing; K.J.S.: conceptualization, formal analysis, funding acquisition, investigation, methodology, validation, visualization, writing—original draft; S.T.: investigation, validation, visualization; Y.J.Z.: investigation, methodology, visualization; L.S.L.: methodology, visualization; X.Y.Y.: investigation, methodology; S.D.: investigation; J.M.C.M.: investigation; A.M.-V.: supervision, writing—review and editing; A.M.: supervision, writing—review and editing; R.R.: funding acquisition, project administration, supervision, writing—original draft, writing—review and editing.

All authors gave final approval for publication and agreed to be held accountable for the work performed therein.

Conflict of interest declaration. We declare we have no competing interests.

Funding. This work was supported by U.S. National Science Foundation GRFP DGE 2139899 to J.M.C.M., by U.S. National Science Foundation grants IOS-2128164 and DEB-2242865 to R.R., Rand Wilbur V. Harlan Research Fellowship to L.S.L. and the Ministry of Education (MOE) Singapore award MOE T2EP30222-0017 to C.F. and A.M.

Acknowledgements. This work features the undergraduate thesis research of K.J.S., and we would like to thank the Cornell MBG-GGD honours thesis program participants for support and feedback on the project.

References

1. Finet C. 2024 Developmental genetics of cuticular micro- and nano-structures in insects. *Curr. Opin. Insect Sci.* **65**, 101254. (doi:10.1016/j.cois.2024.101254)
2. Zhang L, Mazo-Vargas A, Reed RD. 2017 Single master regulatory gene coordinates the evolution and development of butterfly color and iridescence. *Proc. Natl Acad. Sci. USA* **114**, 10707–10712. (doi:10.1073/pnas.1709058114)
3. Thayer RC, Allen FI, Patel NH. 2020 Structural color in *Junonia* butterflies evolves by tuning scale lamina thickness. *eLife* **9**, e52187. (doi:10.7554/eLife.52187)
4. Livraghi L *et al*. 2025 Genetic basis of an adaptive polymorphism controlling butterfly silver iridescence. *Curr. Biol.* **35**, 2475–2477. (doi:10.1016/j.cub.2025.04.042)
5. Ficarrotta V. 2022 A genetic switch for male UV-iridescence in an incipient species pair of sulphur butterflies. *Proc. Natl Acad. Sci. USA* **119**, e2109255118. (doi:10.1101/2021.05.21.445125)
6. Rodriguez-Caro F *et al*. 2021 Novel *Doublesex* duplication associated with sexually dimorphic development of dogface butterfly wings. *Mol. Biol. Evol.* **38**, 5021–5033. (doi:10.1093/molbev/msab228)
7. Prakash A, Finet C, Banerjee TD, Saranathan V, Monteiro A. 2022 Antennapedia and optix regulate metallic silver wing scale development and cell shape in *Bicyclus anynana* butterflies. *Cell Rep.* **40**, 111052. (doi:10.1016/j.celrep.2022.111052)

8. Prakash A, Dion E, Banerjee TD, Monteiro A. 2024 The molecular basis of scale development highlighted by a single-cell atlas of *Bicyclus anynana* butterfly pupal forewings. *Cell Rep.* **43**, 114147. (doi:10.1016/j.celrep.2024.114147)
9. Kerner P, Ikmi A, Coen D, Vervoort M. 2009 Evolutionary history of the iroquois/Irx genes in metazoans. *BMC Evol. Biol.* **9**, 74. (doi:10.1186/1471-2148-9-74)
10. Setton EVW, Ballesteros JA, Blaszczyk PO, Klementz BC, Sharma PP. 2024 A taxon-restricted duplicate of Iroquois3 is required for patterning the spider waist. *PLoS Biol.* **22**, e3002771. (doi:10.1371/journal.pbio.3002771)
11. Chatterjee M, Yu XY, Brady NK, Hatto GC, Amendola CA, Reed RD. 2025 *mirror* determines the far posterior domain in butterfly wings. *eLife* **13**, RP96904. (doi:10.7554/eLife.96904.2)
12. Gomez-Skarmeta JL, Diez del Corral R, de la Calle-Mustienes E, Ferré-Marcó D, Modolell J. 1996 *araucan* and caupolican, two members of the novel *Iroquois* complex, encode homeoproteins that control proneural and vein-forming genes. *Cell* **85**, 95–105. (doi:10.1016/s0092-8674(00)81085-5)
13. Gómez-Skarmeta JL, Modolell J. 1996 *araucan* and caupolican provide a link between compartment subdivisions and patterning of sensory organs and veins in the *Drosophila* wing. *Genes Dev.* **10**, 2935–2945. (doi:10.1101/gad.10.22.2935)
14. Kehl BT, Cho KO, Choi KW. 1998 *mirror*, a *Drosophila* homeobox gene in the *Iroquois* complex, is required for sensory organ and alula formation. *Development* **125**, 1217–1227. (doi:10.1242/dev.125.7.1217)
15. Cavodeassi F, Modolell J, Gómez-Skarmeta JL. 2001 The *Iroquois* family of genes: from body building to neural patterning. *Development* **128**, 2847–2855. (doi:10.1242/dev.128.15.2847)
16. Ikmi A, Netter S, Coen D. 2008 Prepatterning the *Drosophila* notum: the three genes of the *Iroquois* complex play intrinsically distinct roles. *Dev. Biol.* **317**, 634–648. (doi:10.1016/j.ydbio.2007.12.034)
17. Hines HM, Papa R, Ruiz M, Papanicolaou A, Wang C, Nijhout H, McMillan W, Reed RD. 2012 Transcriptome analysis reveals novel patterning and pigmentation genes underlying *Heliconius* butterfly wing pattern variation. *BMC Genomics* **13**, 288. (doi:10.1186/1471-2164-13-288)
18. Fandino RA, Brady NK, Chatterjee M, McDonald JMC, Livraghi L, van der Burg KRL, Mazo-Vargas A, Markenscoff-Papadimitriou E, Reed RD. 2024 The ivory lncRNA regulates seasonal color patterns in buckeye butterflies. *Proc. Natl Acad. Sci. USA* **121**, e2403426121. (doi:10.1101/2024.02.09.579733)
19. Zhang L, Reed RD. 2017 A practical guide to CRISPR/Cas9 genome editing in Lepidoptera. In *Diversity and evolution of butterfly wing patterns: an integrative approach* (eds T Sekimura, HF Nijhout), pp. 155–172. Singapore: Springer Singapore. (doi:10.1007/978-981-10-4956-9_8)
20. Maia R, Gruson H, Endler JA, White TE. 2019 pavo 2: new tools for the spectral and spatial analysis of colour in R. *Methods Ecol. Evol.* **10**, 1097–1107. (doi:10.1111/2041-210X.13174)
21. Ren A, Day CR, Hanly JJ, Counterman BA, Morehouse NI, Martin A. 2020 Convergent evolution of broadband reflectors underlies metallic coloration in butterflies. *Front. Ecol. Evol.* **8**, 206. (doi:10.3389/fevo.2020.00206)
22. Schindelin J *et al*. 2012 Fiji: an open-source platform for biological-image analysis. *Nat. Methods* **9**, 676–682. (doi:10.1038/nmeth.2019)
23. Villinger C, Gregorius H, Kranz C, Höhn K, Münzberg C, Wichert G, Mizaikoff B, Wanner G, Walther P. 2012 FIB/SEM tomography with TEM-like resolution for 3D imaging of high-pressure frozen cells. *Histochem. Cell Biol.* **138**, 549–556. (doi:10.1007/s00418-012-1020-6)
24. Pinheiro J, Bates D. 1999 nlme: linear and nonlinear mixed effects models. (doi:10.32614/cran.package.nlme). See https://CRAN.R-project.org/package=nlme [1, 2, 3.
25. Matsuoka Y, Monteiro A. 2018 Melanin pathway genes regulate color and morphology of butterfly wing scales. *Cell Rep.* **24**, 56–65. (doi:10.1016/j.celrep.2018.05.092)
26. Finet C, Ruan Q, Bei YY, You En Chan J, Saranathan V, Yang JKW, Monteiro A. 2023 Multi-scale dissection of wing transparency in the clearwing butterfly *Phanus vitreus*. *J. R. Soc. Interface* **20**, 20230135. (doi:10.1098/rsif.2023.0135)
27. Banerjee TD, Finet C, Seah KS, Monteiro A. 2024 Optix regulates nanomorphology of butterfly scales primarily via its effects on pigmentation. *Front. Ecol. Evol.* **12**, 1392050. (doi:10.3389/fevo.2024.1392050)
28. Jessop AL, Pirih P, Wang L, Patel NH, Clode PL, Schröder-Turk GE, Wilts BD. 2024 Elucidating nanostructural organization and photonic properties of butterfly wing scales using hyperspectral microscopy. *J. R. Soc. Interface* **21**, 20240185. (doi:10.1098/rsif.2024.0185)
29. Giraldo MA, Stavenga DG. 2016 Brilliant iridescence of *Morpho* butterfly wing scales is due to both a thin film lower lamina and a multilayered upper lamina. *J. Comp. Physiol. A Neuroethol. Sens. Neural. Behav. Physiol.* **202**, 381–388. (doi:10.1007/s00359-016-1084-1)
30. Finet C, Ruan Q, Bei YY, Saranathan V, Monteiro A. 2024 Ridge and crossrib height of butterfly wing scales is a toolbox for structural color diversity. *Biorxiv* (doi:10.1101/2024.03.28.585318)
31. Giraldo MA, Yoshioka S, Liu C, Stavenga DG. 2016 Coloration mechanisms and phylogeny of *Morpho* butterflies. *J. Exp. Biol.* **219**, 3936–3944. (doi:10.1242/jeb.148726)
32. Siddique RH, Vignolini S, Bartels C, Wacker I, Hölscher H. 2016 Colour formation on the wings of the butterfly *Hypolimnas salmacis* by scale stacking. *Sci. Rep.* **6**, 36204. (doi:10.1038/srep36204)
33. Reed RD, Chen PH, Frederik Nijhout H. 2007 Cryptic variation in butterfly eyespot development: the importance of sample size in gene expression studies. *Evol. Dev.* **9**, 2–9. (doi:10.1111/j.1525-142X.2006.00133.x)
34. Oliver JC, Tong XL, Gall LF, Piel WH, Monteiro A. 2012 A single origin for nymphalid butterfly eyespots followed by widespread loss of associated gene expression. *PLoS Genet.* **8**, e1002893. (doi:10.1371/journal.pgen.1002893)
35. Reed RD, Selegue JE, Zhang L, Brunetti CR. 2020 Transcription factors underlying wing margin color patterns and pupal cuticle markings in butterflies. *EvoDevo* **11**, 10. (doi:10.1186/s13227-020-00155-w)
36. Dinwiddie A, Null R, Pizzano M, Chuong L, Leigh Krup A, Ee Tan H, Patel NH. 2014 Dynamics of F-actin prefigure the structure of butterfly wing scales. *Dev. Biol.* **392**, 404–418. (doi:10.1016/j.ydbio.2014.06.005)
37. Thayer RC, Patel NH. 2023 A meta-analysis of butterfly structural colors: their color range, distribution and biological production. *J. Exp. Biol.* **226**, b245940. (doi:10.1242/jeb.245940)
38. Stavenga DG, Leertouwer HL, Wilts BD. 2014 Coloration principles of nymphaline butterflies - thin films, melanin, ommochromes and wing scale stacking. *J. Exp. Biol.* **217**, 2171–2180. (doi:10.1242/jeb.098673)
39. Wasik BR, Liew SF, Lilien DA, Dinwiddie AJ, Noh H, Cao H, Monteiro A. 2014 Artificial selection for structural color on butterfly wings and comparison with natural evolution. *Proc. Natl Acad. Sci. USA* **111**, 12109–12114. (doi:10.1073/pnas.1402770111)
40. Zhang L, Reed RD. 2016 Genome editing in butterflies reveals that *spalt* promotes and *distal-less* represses eyespot colour patterns. *Nat. Commun.* **7**, 11769. (doi:10.1038/ncomms11769)
41. Weatherbee SD, Nijhout HF, Grunert LW, Halder G, Galant R, Selegue J, Carroll S. 1999 *ultrabithorax* function in butterfly wings and the evolution of insect wing patterns. *Curr. Biol.* **9**, 109–115. (doi:10.1016/s0960-9822(99)80064-5)

42. Tendolkar A, Pomerantz AF, Heryanto C, Shirk PD, Patel NH, Martin A. 2021 *ultrabithorax* is a micromanager of hindwing identity in butterflies and moths. *Front. Ecol. Evol.* **9**, 643661. (doi:10.3389/fevo.2021.643661)
43. Tong X, Hrycaj S, Podlaha O, Popadic A, Monteiro A. 2014 Over-expression of *ultrabithorax* alters embryonic body plan and wing patterns in the butterfly *Bicyclus anynana*. *Dev. Biol.* **394**, 357–366. (doi:10.1016/j.ydbio.2014.08.020)
44. Tendolkar A, Mazo-Vargas A, Livraghi L, Hanly JJ, Horne KC, Gilbert LE. 2024 *Cis*-regulatory modes of ultrabithorax inactivation in butterfly forewings. *eLife* **12**, RP90846. (doi:10.7554/eLife.90846)
45. Chatterjee M, Finet C, Monteiro A, Reed R. 2025 Data from: *araucan* regulates butterfly wing iridescence by coordinating scale structure and pigmentation. Dryad Digital Repository. (doi:10.5061/dryad.rfj6q57n6)
46. Chatterjee M *et al*. 2026 Supplementary material from: *araucan* regulates butterfly wing iridescence by coordinating scale structure and pigmentation. Figshare. (doi:10.6084/m9.figshare.c.8420607)